NASA TECHNICAL NOTE

NASA TN D-4891

C.1

NASA TN D-4891

LOAN COPY: RETURN TO
AFWL (WLIL-2)
KIRTLAND AFB, N MEX

PREDICTION OF LIFT AND DRAG FOR SLENDER SHARP-EDGE DELTA WINGS IN GROUND PROXIMITY

by Charles H. Fox, Jr.

Langley Research Center
Langley Station, Hampton, Va.

NATIONAL AERONAUTICS AND SPACE ADMINISTRATION • WASHINGTON, D. C. • JANUARY 1969

TECH LIBRARY KAFB, NM
0131595

PREDICTION OF LIFT AND DRAG FOR SLENDER SHARP-EDGE DELTA WINGS IN GROUND PROXIMITY

By Charles H. Fox, Jr.

Langley Research Center
Langley Station, Hampton, Va.

NATIONAL AERONAUTICS AND SPACE ADMINISTRATION

For sale by the Clearinghouse for Federal Scientific and Technical Information
Springfield, Virginia 22151 – CFSTI price $3.00

PREDICTION OF LIFT AND DRAG FOR SLENDER SHARP-EDGE DELTA WINGS IN GROUND PROXIMITY

By Charles H. Fox, Jr.
Langley Research Center

SUMMARY

A method of predicting the lift and drag of slender planar sharp-edge delta wings in ground proximity is described, and the results are compared with experimental data. The method utilizes a vortex-lattice computer program incorporating an image technique to compute the potential-flow normal-force and axial-force characteristics of delta wings in ground proximity. A recently published vortex-lift concept in free air based on a leading-edge-suction analogy is utilized, and a method is presented for combining it with the results of the potential-flow theory in ground proximity. A comparison of the theoretical and experimental lift and drag for delta wings with a wide range of aspect ratios is presented at selected angles of attack. The comparison indicates that this method provides a reasonably good prediction of the lift and drag in ground proximity for aspect ratios less than 2.0 in the angle-of-attack range from 5° to 16°.

INTRODUCTION

In the design of aircraft, consideration of the effect of ground proximity on the aerodynamic characteristics of the aircraft is always important. If not considered, ground effect may produce large unexpected alterations in the characteristics of the aircraft during landing and take-off. Therefore, methods for the accurate prediction of the aerodynamic characteristics of low-aspect-ratio delta wings in ground proximity are necessary to the aircraft designer. The present study is concerned with delta-wing planforms for which the proximity of the ground considerably alters the aerodynamic characteristics of the aircraft. (See ref. 1.) The results are only applicable to aircraft having delta wings with sharp leading edges, low aspect ratios, and slender planar airfoil sections. In this study, only the isolated wing is considered.

Classical potential-flow theory as implemented by lifting-line and horseshoe-vortex methods (for example, see ref. 2) has proven inadequate to predict the lift and drag of the low-aspect-ratio sharp-leading-edge delta-wing planform irrespective of the presence of the ground. One reason for this inadequacy is the failure of these methods to treat the chordwise variation of lift. Lifting-surface theory implemented by vortex-lattice methods

(for example, refs. 3 and 4) was developed in order to include the chordwise lift distributions; however, even this technique is inadequate to treat the present planform. The basic reason for these inadequacies is that classical potential-flow theory assumes completely attached flow whereas, in reality, the flow separates from the leading edges and forms spiral vortices which result in a loss of leading-edge suction and an increase in lift. Reference 5 presents a new concept for the calculation of the vortex lift of planar sharp-leading-edge delta wings based on a leading-edge-suction analogy. This concept provides a reasonably accurate method of predicting the total lift of planar sharp-leading-edge delta wings in free air.

The present study employs a vortex-lattice potential-flow-theory lifting-surface method incorporating an image technique to represent the wing in ground proximity; a method is also introduced for combining the potential-flow theory with the free-air vortex-lift concept. The resulting theory yields a reasonably good prediction of the total lift and drag of planar sharp-edge delta wings in ground proximity. The method is not applicable to the prediction of pitching moment, which is not considered herein.

SYMBOLS

Longitudinal data are presented about the stability axes.

AR	aspect ratio, b^2/S
b	total wing span, feet (meters)
C_A	axial-force coefficient, positive direction is toward trailing edge, $\frac{\text{Axial force}}{qS}$
$C_{A,der}$	axial-force coefficient derived from $C_{N,lat}$, $C_{A,lat}$, and $\frac{\partial C_{Di}}{\partial C^2_{L,lat}}$
C_D	drag coefficient, $\frac{\text{Drag}}{qS}$
C_L	lift coefficient, $\frac{\text{Lift}}{qS}$
C_N	normal-force coefficient, positive direction is away from ground plane, $\frac{\text{Normal force}}{qS}$
K	a free-air proportional correction to vortex-lattice axial-force coefficient defined as $\frac{C_{A,der}}{C_{A,lat}}$
q	dynamic pressure, pounds/foot^2 (newtons/meter^2)

S	wing reference area, feet^2 (meters^2)
$\frac{h_{\bar{c}/4}}{\bar{c}}$	normalized height parameter, height of local quarter-chord point of mean aerodynamic chord above ground divided by mean aerodynamic chord
$\frac{\partial C_{Di}}{\partial C^2_{L,lat}}$	induced-drag factor
α	angle of attack, degrees
Λ	leading-edge sweep angle, degrees

Subscripts:

lat	results of potential-flow theory vortex-lattice computer program
pot	potential-flow theory using $C_{A,der}$
t	total

METHOD OF ANALYSIS

A vortex-lattice method of calculating the potential-flow aerodynamic characteristics of delta wings was programed for solution on a high-speed computer. In this method, the wing is subdivided in both the spanwise and chordwise directions into a number of elemental areas. In the present study, six spanwise and six chordwise divisions were used on each half of the wing. The local chord was divided into six equal increments whereas the spanwise divisions placed trailing-vortex legs at 0, 14, 28, 42, 56, 70, and 100 percent of the semispan. Each elemental area is represented by a horseshoe vortex with the bound portion lying along the local quarter-chord line of the element. The boundary condition that the flow be tangential to the wing surface is then satisfied for each element at a point on the lateral midpoint of the local three-quarter-chord line of the element.

The proximity of the ground is represented in the computer program by a mirror image of the vortex-lattice system of the wing across the ground plane. The system composed of the vortex lattice representing the wing and the vortex lattice representing the image wing is used to compute the aerodynamic characteristics of the wing in ground proximity.

In the vortex-lattice program, the induced velocity at a given point is related to the circulation strength of a given horseshoe vortex through a geometric-influence coefficient given by the Biot-Savart law. (See ref. 6, pp. 126-128.) In this program, the geometric-influence coefficients are computed, the boundary condition is applied, and the

circulation strengths are calculated. These circulation strengths are used to obtain the total velocities at the midpoints of the vortex-line segments. The total velocities are then used to compute the normal and axial forces acting on the wing. The computer program provides the potential-flow-theory normal and axial forces corresponding to selected conditions of ground height and angle of attack for the specified wing planform. The results are presented in this paper as a function of a nondimensional height parameter, given as the height of the quarter-mean-aerodynamic-chord point above the ground divided by the mean aerodynamic chord.

The computer program used herein was designed for wings of arbitrary planform. At the present time, however, this program has only been verified for computing $C_{N,lat}$, $C_{A,lat}$, and $\frac{\partial C_{Di}}{\partial C^2_{L,lat}}$ for delta-planform wings. Therefore, the complete program is not described in detail herein, and it is not available for release at this time. However, a brief description of the equations used in this computer program is included in the appendix.

An axial-force coefficient $C_{A,lat}$ can be calculated by using the vortex-lattice method as implemented herein since the total velocities used to compute the forces on the vortex lines were calculated at the midpoint of each vortex segment rather than at the control point where the boundary condition was applied. However, the values obtained are somewhat inaccurate because of the discrete nature of the vortex-lattice formulation of the problem. The first task is, therefore, the correction of the axial-force coefficient. The method used herein relies on the fact that the vortex-lattice span load distribution in free air can be used to compute an accurate value of the induced-drag factor $\frac{\partial C_{Di}}{\partial C^2_{L,lat}}$.

The accuracy of this calculation has been checked by independent methods. (See ref. 7.) Thus, a better approximation of the free-air axial-force coefficient, valid for large angles of attack in potential flow, is obtained from the solution of

$$\left.\begin{aligned} -C_{A,der} &= C_{L,lat} \sin\alpha - \frac{\partial C_{Di}}{\partial C^2_{L,lat}} C^2_{L,lat} \cos\alpha \\ C_{L,lat} &= C_{N,lat} \cos\alpha - C_{A,der} \sin\alpha \end{aligned}\right\} \tag{1}$$

The corrected axial-force coefficient in free air may be written in terms of the vortex-lattice axial-force coefficient as

$$C_{A,der} = KC_{A,lat} \tag{2}$$

Equation (2) defines K, the fractional correction to the axial-force coefficient in free air. For a given wing planform, K is assumed to be a function of angle of attack but not a function of height above the ground.

The lift and drag coefficients are obtained by resolving the normal- and axial-force coefficients in directions perpendicular and parallel to the free stream. If the results of the vortex-lattice program are used directly, the lift and drag coefficients are

$$\left.\begin{aligned} C_{L,lat} &= C_{N,lat} \cos \alpha - C_{A,lat} \sin \alpha \\ C_{D,lat} &= C_{N,lat} \sin \alpha + C_{A,lat} \cos \alpha \end{aligned}\right\} \tag{3}$$

The effect of introducing K is to replace equations (3) by

$$\left.\begin{aligned} C_{L,pot} &= C_{N,lat} \cos \alpha - KC_{A,lat} \sin \alpha \\ C_{D,pot} &= C_{N,lat} \sin \alpha + KC_{A,lat} \cos \alpha \end{aligned}\right\} \tag{4}$$

In this paper, equations (3) are referred to as the vortex-lattice theory, and equations (4) are referred to as the potential theory.

The vortex-lift concept developed in reference 5 for planar sharp-leading-edge delta wings is based on a leading-edge-suction analogy. For a planar sharp-leading-edge delta wing, the leading-edge suction is lost, and a leading-edge spiral vortex is formed. (See ref. 5.) In addition, the equilibrium force required to maintain the spiral vortex adds an increment to the normal force which is identical in magnitude to the lost leading-edge suction. By using the vortex-lattice method to account for the effect of the ground on the leading-edge suction, the total lift coefficient can be expressed as

$$C_{L,t} = \left(C_{N,lat} + \frac{K\left|C_{A,lat}\right|}{\cos \Lambda}\right)\cos \alpha \tag{5a}$$

Since the leading edge is sharp, no leading-edge suction is developed (that is, no force is developed in the axial direction); therefore, the total free-air drag coefficient is

$$C_{D,t} = C_{L,t} \tan \alpha \tag{5b}$$

Equations (5) are referred to herein as the present theory.

RESULTS AND DISCUSSION

Several features of the analysis should be noted. First, the existence of the spiral vortices emanating from the leading edge implies a redistribution of vorticity in the wing

and wake. This redistribution is not accounted for with respect to the image wing below the ground plane, even though the results of reference 5 have been used to correct for this effect at the real wing. Secondly, the choice of the coordinate system used in the vortex-lattice program described in the appendix leads to a wake which, at positive angles of attack, intersects and passes through the ground plane. Finally, since the present approach uses the method of reference 5, which does not predict the distribution of forces over the wing, this approach cannot be used to calculate pitching moment.

In view of the assumptions used in developing the present theory, the justification for its use must rest primarily upon a comparison with experimental data. One of the most complete experimental studies of ground effect for sharp-edged delta wings is that of reference 8, in which a series of wings with leading-edge sweep angles of 75°, 70°, 60°, and 50° (aspect ratios of 1.072, 1.456, 2.309, and 3.356, respectively) were tested. These wings were tested by using both the fixed-ground-board and image-model test methods at a free-stream velocity of 114.8 ft/sec (35.0 m/sec) mounted on a strut support. Certain unexplained nonlinearities existed at low angles of attack in the data of reference 8; however, the data were self-consistent. Corresponding with the assumptions of the theory, the wings were isolated; that is, there was no fuselage or tail. The experimental data are presented in terms of the height parameter used in the present study.

The lift and drag characteristics of the wings as functions of normalized ground height are presented in figure 1 for $\alpha = 10^{\circ}$ and in figure 2 for $\alpha = 15^{\circ}$. The drag coefficients presented in these figures do not include the friction-drag component which has been removed by subtracting the minimum drag coefficients from the data of reference 8. (The values subtracted were 0.008, 0.010, 0.011, and 0.012 for wings with leading-edge sweeps of 75°, 70°, 60°, and 50°, respectively.)

An examination of figures 1 and 2 reveals that when either the potential theory or the present theory is able to predict the free-air lift coefficients, it can also be used to predict the effect of ground proximity reasonably well. For aspect ratios less than 2.0, where the leading-edge vortex is well developed, the present theory (eqs. (5)) accurately predicts the lift. As the aspect ratio increases and the effects of the leading-edge vortex become less pronounced, the accuracy of the potential-theory lift predictions (eqs. (4)) becomes progressively better and that of the present-theory predictions becomes worse. In general, the present theory yields a better drag prediction than the potential theory. These effects can also be seen in figures 3 and 4 which summarize the lift and drag characteristics as functions of aspect ratio for selected ground heights.

In order to examine the effects of angle of attack over a larger range, the data of reference 9 were used. Reference 9 presents tabulated lift and drag data as functions of angle of attack and ground height for a wing with an aspect ratio of 1.616 ($\Lambda = 68^{\circ}$). The wing was suspended on a wire support rig over a fixed ground board and tested at a

free-stream velocity of 120 ft/sec (36.6 m/sec). A minimum drag coefficient of 0.009 was subtracted from the measured drag data of reference 9 in order to eliminate friction drag from the data.

The results of the theoretical calculations for a wing with an aspect ratio of 1.616 are compared with the data of reference 9 over an angle-of-attack range from 1° to 15.55° in figure 5. The comparison is further summarized in figure 6. Note that figures 3 and 4 indicate that the present theory should yield a good prediction of the lift and drag at this aspect ratio. The data from reference 9 indicate that the same result is obtained except at an angle of attack of 1°. It should be noted, however, that an angle of attack of 1° probably does not provide sufficient leading-edge separation for the complete formation of the leading-edge spiral-vortex system. Other than this anomalous point, the present theory gives a good prediction of the lift and drag for each angle of attack throughout the ground-height range. The predicted lift and drag are presented in figure 6 as a function of angle of attack for selected ground heights. The present theory yields a reasonably good prediction of the lift and drag throughout the angle-of-attack range from some angle of attack between 1° and 5.52° up to an angle of attack of 15.55°, the highest angle of attack for which experimental data were available. (See fig. 5.)

CONCLUDING REMARKS

A method of predicting the lift and drag of slender planar sharp-edge delta wings in ground proximity is described, and the results are compared with experimental data. The method utilizes a vortex-lattice computer program incorporating an image technique to compute the potential-flow normal-force and axial-force characteristics of delta wings in ground proximity. A correction to account for finite vortex-lattice spacing is made to the free-air vortex-lattice axial force, and the correction is assumed applicable to the vortex-lattice axial force in ground proximity. A recently published vortex-lift concept in free air based on a leading-edge-suction analogy is utilized, and a method is presented for combining it with the results of the potential-flow theory in ground proximity. A comparison of the theoretical and experimental lift and drag is presented at selected angles of attack for delta wings with a wide range of aspect ratios. This method provides a reasonably good prediction of the lift and drag in ground proximity for aspect ratios less than 2.0 in the angle-of-attack range from approximately 5° to 16°.

Langley Research Center,
National Aeronautics and Space Administration,
Langley Station, Hampton, Va., July 5, 1968,
126-13-01-50-23.

APPENDIX

VORTEX-LATTICE METHOD

The vortex-lattice method used in the present analysis can best be described by giving the basic equations used in the computer program.

Symbols

The following is a list of those symbols used in the appendix which differ from those used in the main text. Any convenient system of measure can be used. The sign conventions used in the present study may differ somewhat from the standard sign conventions.

B	matrix defined by equation (A6)
F_A	axial force, positive toward trailing edge
F_N	normal force, positive away from ground
H	influence coefficient in X,Y,Z coordinate system
H^*	influence coefficient in X^*,Y^*,Z^* coordinate system
h	height of apex of wing above ground
l	length of vortex-line segment on wing
P(x,y,z)	general point in space
s	horseshoe-vortex semispan
U_∞	free-stream velocity, $U_\infty = 1$
u,v,w	perturbation-velocity components in positive X-, Y-, and Z-directions
V	resultant induced velocity with components u, v, and w
X,Y,Z	orthogonal right-handed primary Cartesian coordinate system with origin at wing apex (see fig. 7); positive X-direction is away from trailing edge, positive Y-direction is toward right wing tip, and positive Z-direction is toward ground

APPENDIX

X^*,Y^*,Z^* orthogonal right-handed primary Cartesian coordinate system associated with image wing (see fig. 7(d)); positive X^* is away from trailing edge, positive Y^* is parallel to positive Y, and positive Z^* is away from ground

x,y,z orthogonal right-handed secondary Cartesian coordinate system with origin at lateral midpoint of local quarter chord of element (see fig. 7(b))

x^*,y^*,z^* orthogonal right-handed secondary Cartesian coordinate system associated with image wing

Γ circulation strength

ϕ angle between normal to ground plane and Z-axis (note that $\phi = \alpha$)

ψ angle between bound vortex and y-axis, positive direction is counterclockwise from positive y-axis

Subscripts:

a particular point (P_a)

BC boundary condition

b particular point (P_b)

c chordwise segment

I image wing

l left wing panel

R real or actual wing

r right wing panel

s spanwise segment

u,v,w components of influence coefficient in x-, y-, and z-directions

APPENDIX

Equations Used In Vortex-Lattice Computer Program

Application of the vortex-lattice method to a delta-wing planform is shown in figure 7. A simplified subdivision of a delta wing into elemental parts is shown in figure 7(a). Figure 7(b) shows a horseshoe vortex representing a typical element. The orthogonal primary coordinate system used for the wing is shown in figure 7(c). The height of the wing apex above the ground is h, and the angle between h and the Z-axis is ϕ. The angle of attack α is defined as the angle between the free-stream velocity and the X-axis. To simplify the analysis, the assumption is made that $\phi = \alpha$. Thus, in the present investigation, the dynamic situation of an aircraft landing maneuver in which ϕ and α are independent functions of time is not represented. The perturbation velocities in the X-, Y-, and Z-directions are shown in figure 7(c) as u, v, and w, respectively. The orthogonal secondary coordinate system associated with the horseshoe vortex, representing a typical element of the wing, is shown in figure 7(b). The angle between the bound vortex and the y-axis is defined as ψ. The semispan of the horseshoe vortex is s. Note that a secondary coordinate system is associated with each horseshoe vortex of the lattice.

The basic relation between the induced velocities V and the horseshoe-vortex circulation strengths Γ is, in matrix notation,

$$\{V\} = [H]\{\Gamma\} \tag{A1}$$

where $[H]$ is a geometric-influence-coefficient matrix. In the computer program, this vector equation is replaced by three scalar equations for u, v, and w.

The first task is to compute the influence-coefficient matrix. By using a method similar to reference 6, pages 157-160, the influence of a single horseshoe of unit circulation at a point P(x,y,z) in the secondary coordinate system is

$$H_u(x,y,z) = \left\{\frac{z\cos\psi}{4\pi\left[z^2 + (y\sin\psi - x\cos\psi)^2\right]}\right\}\left[\frac{y\cos\psi + x\sin\psi + \frac{s}{\cos\psi}}{\sqrt{z^2 + (y+s)^2 + (x + s\tan\psi)^2}}\right.$$
$$\left. - \frac{y\cos\psi + x\sin\psi - \frac{s}{\cos\psi}}{\sqrt{z^2 + (y-s)^2 + (x - s\tan\psi)^2}}\right] \tag{A2a}$$

APPENDIX

$$H_V(x,y,z) = \left\{\frac{-z \sin\psi}{4\pi\left[z^2 + (y \sin\psi - x \cos\psi)^2\right]}\right\}\left[\frac{y \cos\psi + x \sin\psi + \frac{s}{\cos\psi}}{\sqrt{z^2 + (y+s)^2 + (x + s \tan\psi)^2}} - \frac{y \cos\psi + x \sin\psi - \frac{s}{\cos\psi}}{\sqrt{z^2 + (y-s)^2 + (x - s \tan\psi)^2}}\right]$$

$$+\left\{\frac{z}{4\pi\left[z^2 + (y-s)^2\right]}\right\}\left[1 + \frac{-x + s \tan\psi}{\sqrt{z^2 + (y-s)^2 + (x - s \tan\psi)^2}}\right]$$

$$+\left\{\frac{-z}{4\pi\left[z^2 + (y+s)^2\right]}\right\}\left[1 + \frac{-x - s \tan\psi}{\sqrt{z^2 + (y+s)^2 + (x + s \tan\psi)^2}}\right] \qquad \text{(A2b)}$$

$$H_W(x,y,z) = \left\{\frac{y \sin\psi - x \cos\psi}{4\pi\left[z^2 + (y \sin\psi - x \cos\psi)^2\right]}\right\}\left[\frac{y \cos\psi + x \sin\psi + \frac{s}{\cos\psi}}{\sqrt{z^2 + (y+s)^2 + (x + s \tan\psi)^2}} - \frac{y \cos\psi + x \sin\psi - \frac{s}{\cos\psi}}{\sqrt{z^2 + (y-s)^2 + (x - s \tan\psi)^2}}\right]$$

$$+\left\{\frac{-(y-s)}{4\pi\left[z^2 + (y-s)^2\right]}\right\}\left[1 + \frac{-x + s \tan\psi}{\sqrt{z^2 + (y-s)^2 + (x - s \tan\psi)^2}}\right]$$

$$+\left\{\frac{y+s}{4\pi\left[z^2 + (y+s)^2\right]}\right\}\left[1 + \frac{-x - s \tan\psi}{\sqrt{z^2 + (y+s)^2 + (x + s \tan\psi)^2}}\right] \qquad \text{(A2c)}$$

Equations (A2) are based on the assumption that the trailing vortex sheet lies in the plane of the wing and extends to infinity. Because this assumption is made, the physical situation in which the trailing vortex sheet essentially follows the free-stream direction is not represented. Nonetheless, this assumption was made in order to simplify the equations.

From considerations of symmetry, for each horseshoe vortex on the left half of the real wing, there exists a corresponding horseshoe vortex on the right half of the real wing as well as on the left and right halves of the image wing, all of which have equal circulation strengths. Therefore, equation (A1) can be restricted to consideration of the left half of the real wing provided each element of the H matrix is the sum of four successive applications of equations (A2) with sets of the secondary coordinates (x,y,z) appropriate to each of the four wing panels being used.

Let $(X_b, Y_b, 0)$ represent the coordinate of a point P_b on the left half of the real wing at which induced velocities are to be computed. Let $(X_a, Y_a, 0)$ be the origin of the secondary coordinate system of a horseshoe vortex on the left half of the real wing. The corresponding element of the influence-coefficient matrix $[H]$ may be written as

$$H = H_{l,R} + H_{r,R} + H_{l,I} + H_{r,I} = H_R + H_I \qquad \text{(A3)}$$

APPENDIX

The u, v, and w components of $H_{l,R}$ are found directly from equations (A2) by letting $y = y_l$ and using

$$x = X_b - X_a$$

$$y_l = Y_b - Y_a$$

$$z = 0$$

Since $H_{r,R}$ is symmetrically related to the influence of the left real horseshoe vortex on a point $(X_b,-Y_b,0)$, let $y_r = -Y_b - Y_a$ and reverse the sign of the component of V in the Y-direction. Then, the components of $H_R = H_{l,R} + H_{r,R}$ are

$$H_{u,R} = H_u(x,y_l,z) + H_u(x,y_r,z) \tag{A4a}$$

$$H_{v,R} = H_v(x,y_l,z) - H_v(x,y_r,z) \tag{A4b}$$

$$H_{w,R} = H_w(x,y_l,z) + H_w(x,y_r,z) \tag{A4c}$$

To determine the image-wing influence terms, the X,Y,Z coordinate system is translated downward through the ground plane and rotated through an angle of 2ϕ in the XZ-plane. (See fig. 7(d).) The assumption that the wake of the real wing lies in the XY-plane results in a wake which, at positive angles of attack, intercepts the ground and passes into the image region below. Similarly, the image wake intercepts the ground and passes into the real region above. Although it is hoped that such behavior will not significantly affect the present results, large errors would probably result if the present technique were used to obtain the downwash at a rear tail. The technique used to form the image in this investigation depends upon the assumption that the wing is planar. The image system would be incorrect if the wing had such nonplanar characteristics as camber, twist, dihedral, or a deflected flap.

With respect to the X^*,Y^*,Z^* coordinate system, the coordinates of the point $(X_b,Y_b,0)$ become (see fig. 7(d))

$$X_b^* = -2h \sin \phi + X_b \cos 2\phi$$

$$Y_b^* = Y_b$$

$$Z_b^* = -2h \cos \phi - X_b \sin 2\phi$$

Thus, to obtain the influence of the left half of the image wing on the left half of the real wing $(H_{l,I})$, use

APPENDIX

$$x^* = -2h \sin \phi + X_b \cos 2\phi - X_a$$

$$y_l{}^* = Y_b - Y_a$$

$$z^* = 2h \cos \phi - X_b \sin 2\phi$$

To obtain the influence of the right half of the image wing on the left half of the real wing, the y-coordinate is altered to

$$y_r{}^* = -Y_b - Y_a$$

and the sign of the v component is reversed.

Substitution of these coordinates into equations (A4) yields the components H_u^*, H_v^*, and H_w^*. These image-influence components are expressed in the directions of the rotated axis system. The following equations are used to resolve the image influence into the X-, Y-, and Z-directions and to account for the fact that the circulation strengths of the image vortices are opposite in sense to those on the real wing:

$$\left[H_I\right] = -\left[H^*\right]\left[B\right] \tag{A5}$$

where

$$H_I = -H_{l,I} + H_{r,I}$$

and the components of the H_I matrix are $H_{u,I}$, $H_{v,I}$, and $H_{w,I}$; the components of the H^* matrix are H_u^*, H_v^*, and H_w^*; and the B matrix is defined as follows:

$$B = \begin{bmatrix} \cos 2\phi & 0 & -\sin 2\phi \\ 0 & 1 & 0 \\ \sin 2\phi & 0 & \cos 2\phi \end{bmatrix} \tag{A6}$$

Since only planar wings are considered in the present study, the boundary condition is

$$w_{BC} - U_\infty \sin \alpha = 0 \tag{A7}$$

or for a free-stream velocity of unity

$$w_{BC} = \sin \alpha \tag{A8}$$

The circulation strengths are then computed from the equation

$$\left\{\Gamma\right\} = \left[H\right]^{-1}\left\{w_{BC}\right\} \tag{A9}$$

where each element of the H matrix is the total influence at a given boundary point caused by a given set of four symmetrically placed vortices on the real and image wings.

Since the circulation strengths are known, computation of the forces acting on the wing is now possible. Let a segment be defined as that portion of a line of vorticity on the wing which has a constant circulation strength. The present analysis computes the induced velocity at the midpoint of each segment from the equation

$$\{V\} = [H]\{\Gamma\} \tag{A10}$$

where the H matrix is now the influence of the set of horseshoe vortices on the set of points composed of the midpoints of the segments. If the induced velocities are expressed in terms of u, v, and w, the forces on the wing can be computed by forming the vector cross product of the circulation strengths of the segments and the induced velocities at the midpoints of the segments. For a spanwise segment, the forces are

$$F_{A,s} = 2\Gamma_s(w_s - \sin\alpha)(2s) \tag{A11a}$$

$$F_{N,s} = 2\Gamma_s\left[v_s \tan\psi - (u_s - \cos\alpha)\right](2s) \tag{A11b}$$

where the subscript s denotes a spanwise segment. For a chordwise segment, the forces are

$$F_{A,c} = 0 \tag{A12a}$$

$$F_{N,c} = 2\Gamma_c v_c l_c \tag{A12b}$$

where the subscript c denotes a chordwise segment, l_c is the segment length contained within the planform, and Γ_c is the net circulation strength resulting from the individual circulations of each trailing-horseshoe-vortex leg forming that segment.

The total normal and axial forces acting on the wing are obtained by summing the normal and axial forces acting on all segments. The values of $C_{N,lat}$ and $C_{A,lat}$ are then computed from the total normal and axial forces. The method of computing $\frac{\partial C_{Di}}{\partial C^2_{L,lat}}$ in free air is given in reference 7.

REFERENCES

1. Kemp, William B., Jr.; Lockwood, Vernard E.; and Phillips, W. Pelham: Ground Effects Related to Landing of Airplanes With Low-Aspect-Ratio Wings. NASA TN D-3583, 1966.

2. Campbell, George S.: A Finite-Step Method for the Calculation of Span Loadings of Unusual Plan Forms. NACA RM L50L13, 1951.

3. Rubbert, Paul E.: Theoretical Characteristics of Arbitrary Wings by a Non-Planar Vortex Lattice Method. Doc. No. D6-9244, Boeing Co., Feb. 1964.

4. Hedman, Sven G.: Vortex Lattice Method for Calculation of Quasi Steady State Loadings on Thin Elastic Wings in Subsonic Flow. FFA Rep. 105, Aeronaut. Res. Inst. Swed., 1966.

5. Polhamus, Edward C.: A Concept of the Vortex Lift of Sharp-Edge Delta Wings Based on a Leading-Edge-Suction Analogy. NASA TN D-3767, 1966.

6. Glauert, H.: The Elements of Aerofoil and Airscrew Theory. Second ed., Cambridge Univ. Press, 1947. (Reprinted 1948.)

7. Lamar, John E.: A Modified Multhopp Approach for Predicting Lifting Pressures and Camber Shape for Composite Planforms in Subsonic Flow. NASA TN D-4427, 1968.

8. Anon.: Ailes Delta de Differentes Fleches et Aile Rectangulaire $\lambda = 2$ – Representation du Sol par la Methode du Plancher et par la Methode de l'Image. O.N.E.R.A. P.V. No. 13/2449.A, Oct. 1963.

9. Kirkpatrick, D. L. I.: Experimental Investigation of the Ground Effect on the Subsonic Longitudinal Characteristics of a Delta Wing of Aspect Ratio 1.616. Tech. Rep. No. 66179, Brit. R.A.E., June 1966.

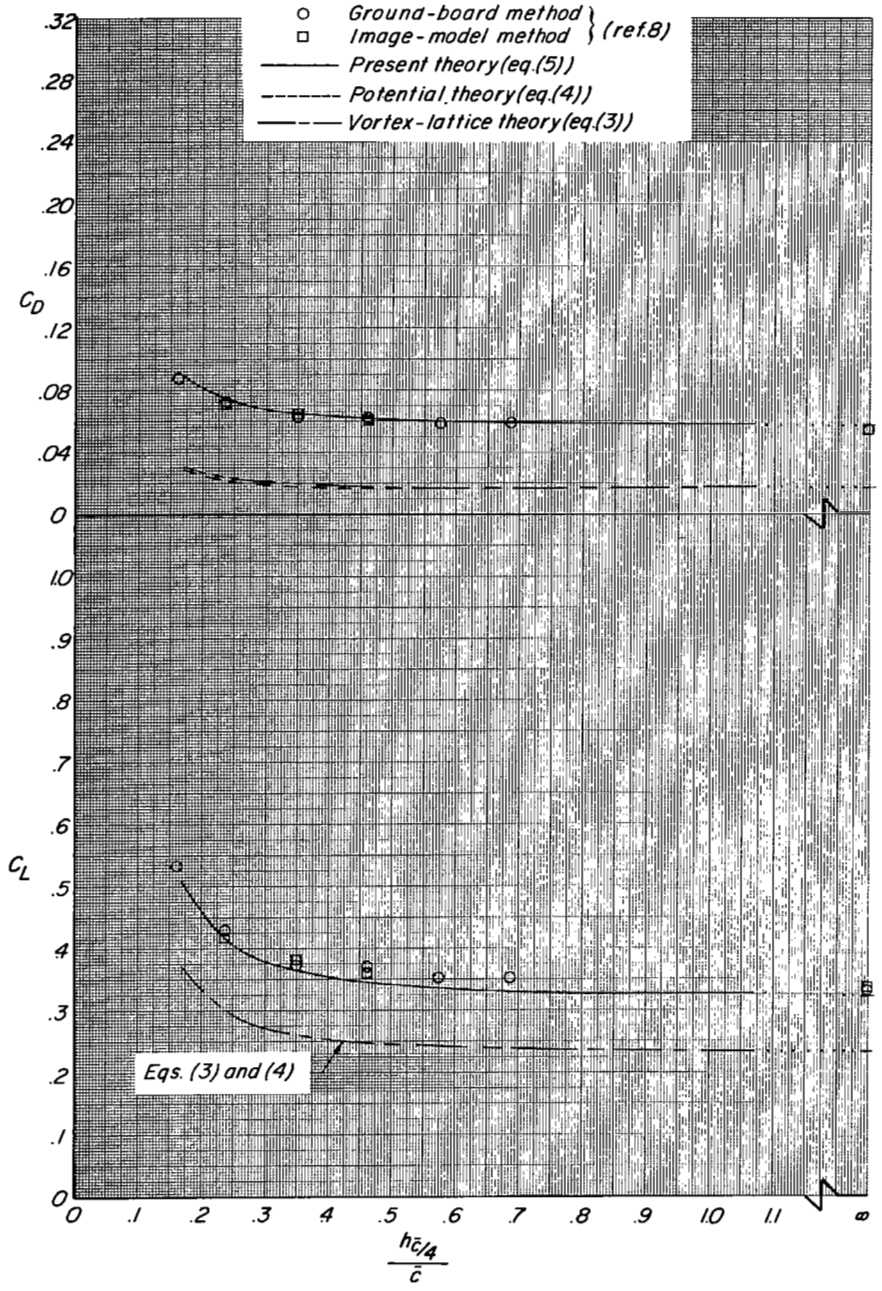

(a) $\Lambda = 75^0$; AR = 1.072.

Figure 1.- Comparison of lift and drag coefficients determined by different theories with the experimental data of reference 8 at an angle of attack of 10^0.

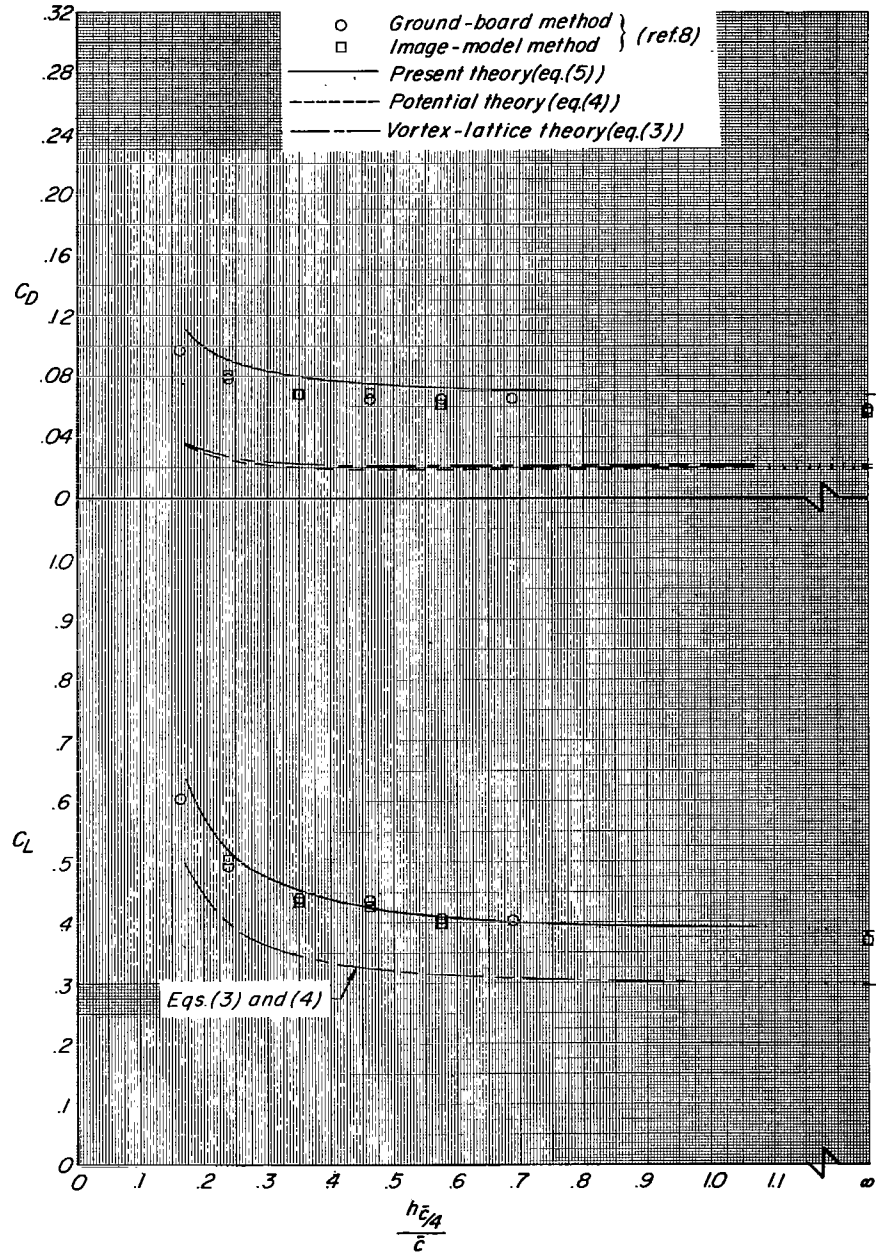

(b) $\Lambda = 70^0$; AR = 1.456.

Figure 1.- Continued.

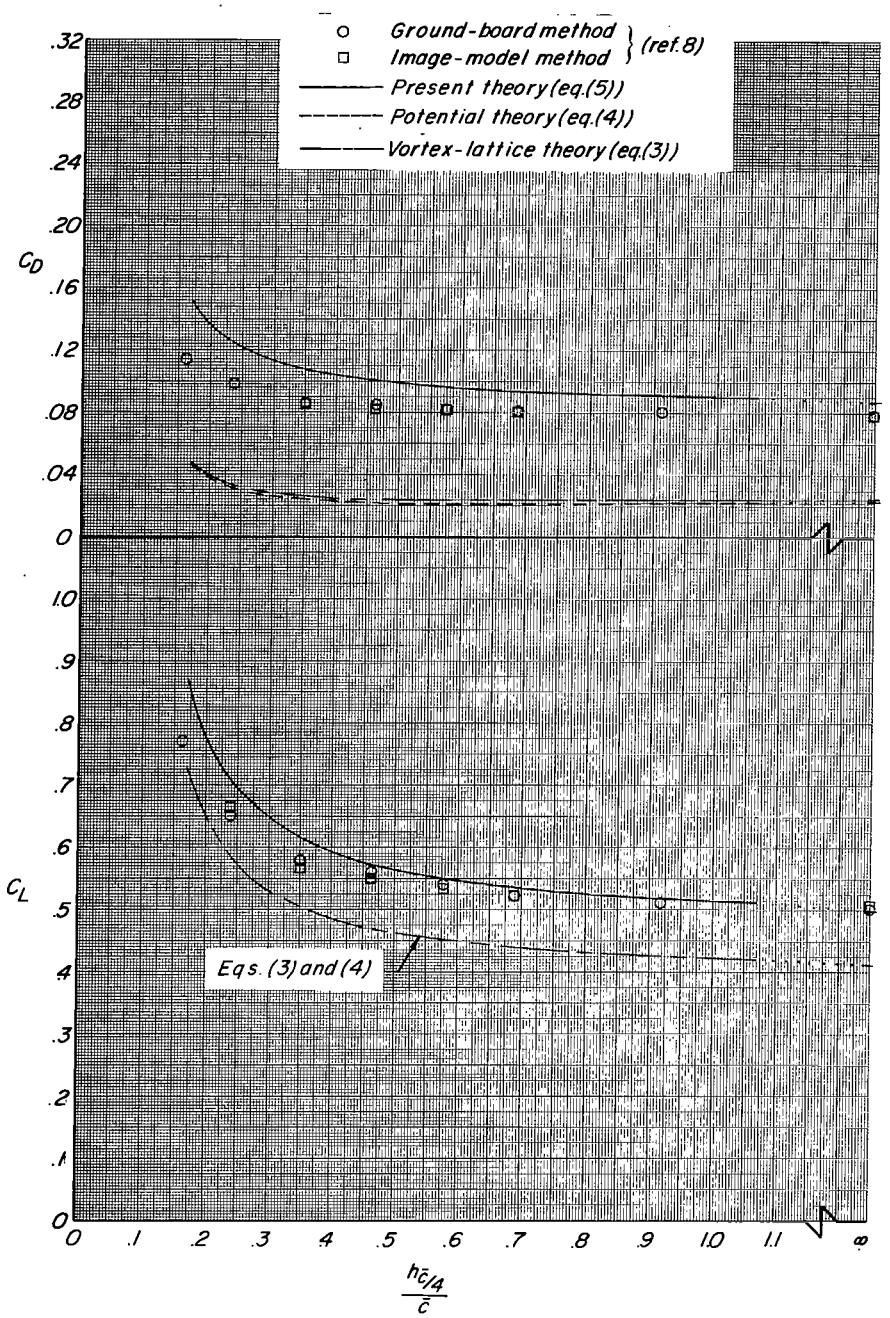

(c) $\Lambda = 60^0$; AR = 2.309.

Figure 1.- Continued.

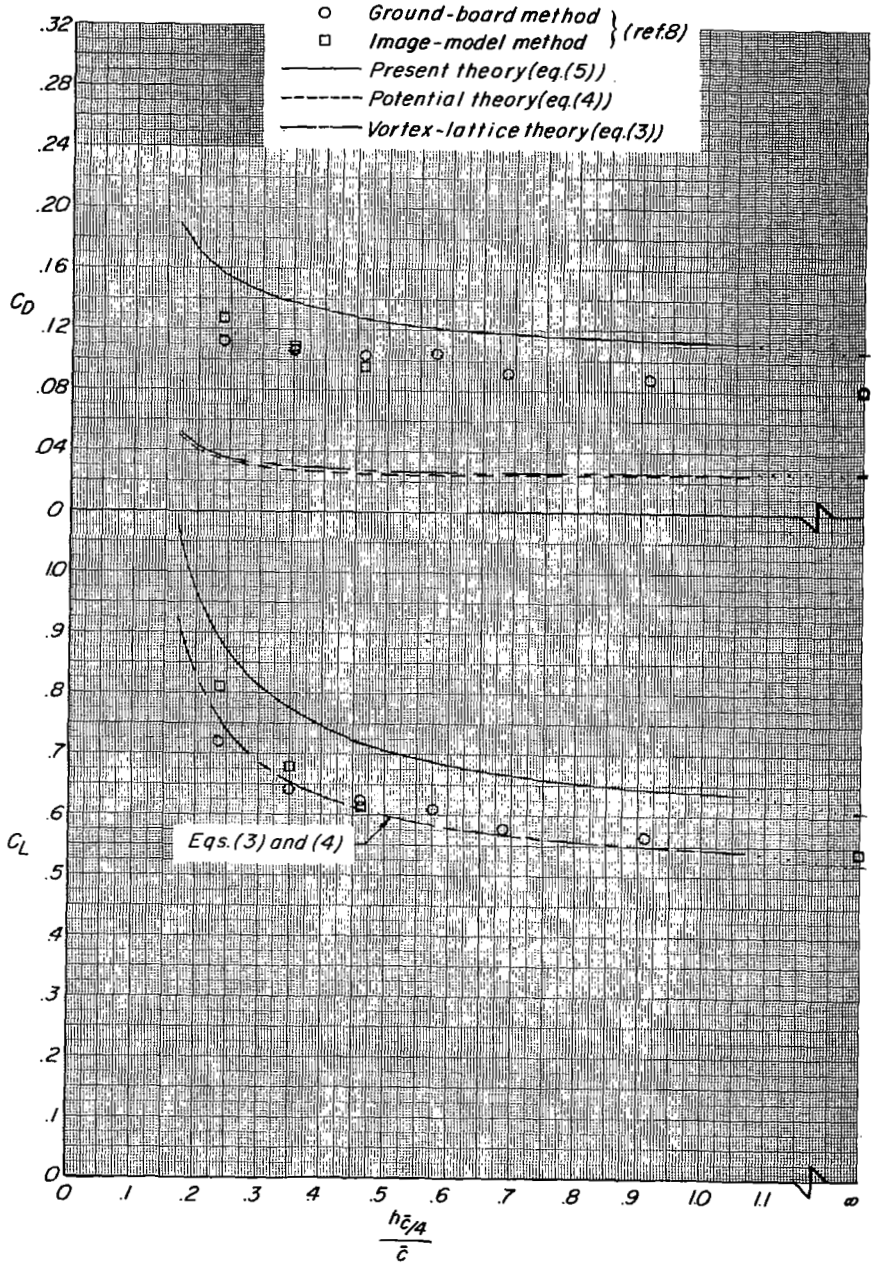

(d) $\Lambda = 50^0$; AR = 3.356.

Figure 1.- Concluded.

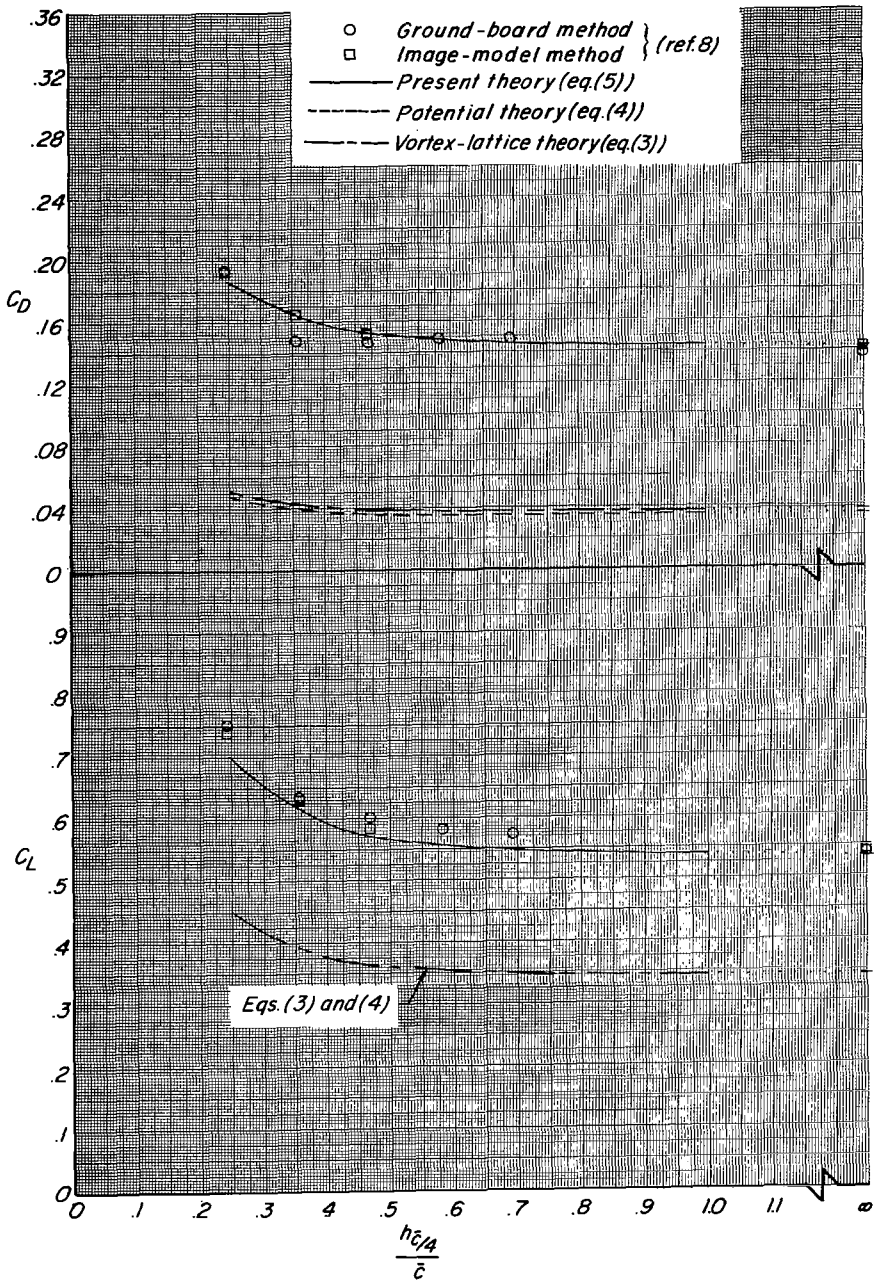

(a) $\Lambda = 75^{\circ}$; AR = 1.072.

Figure 2.- Comparison of lift and drag coefficients determined by different theories with the experimental data of reference 8 at an angle of attack of 15°.

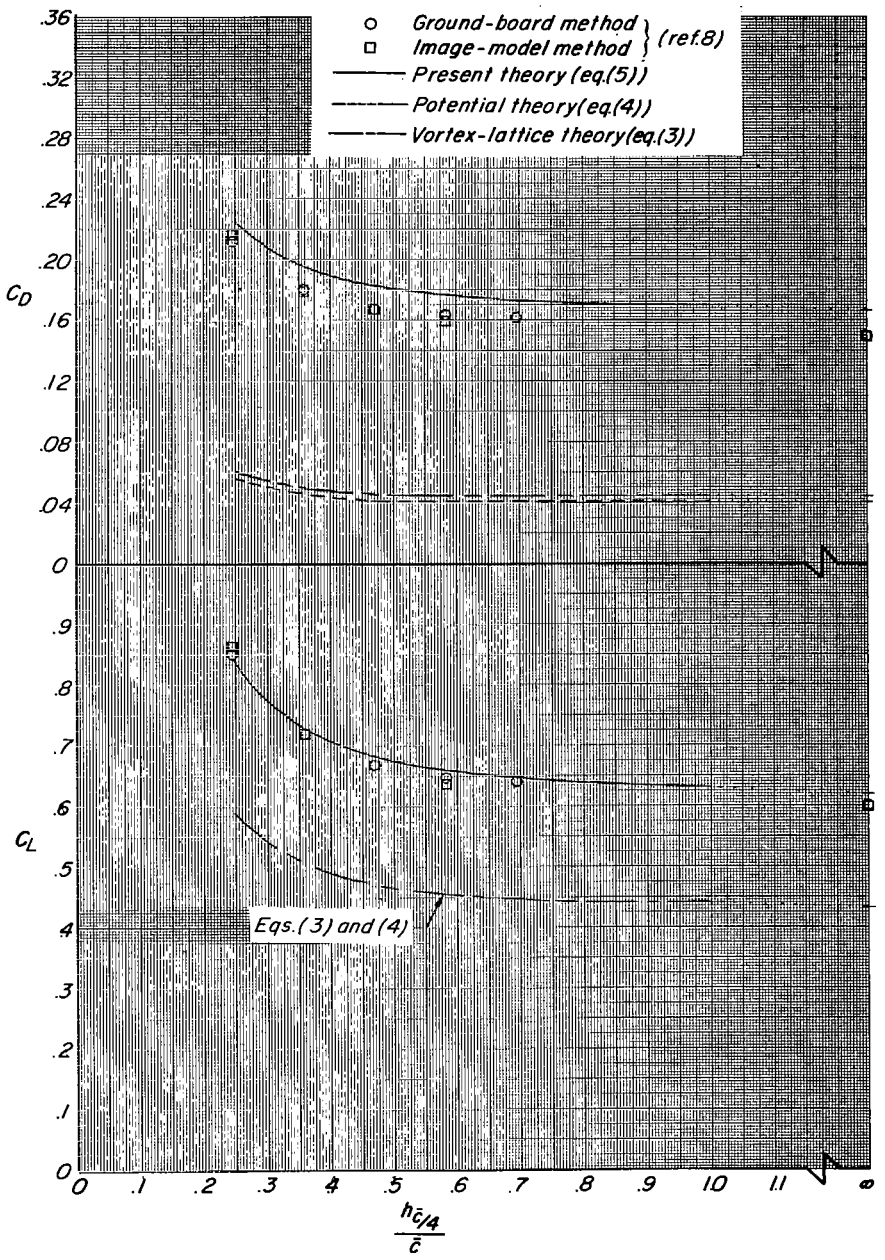

(b) $\Lambda = 70^0$; AR = 1.456.

Figure 2.- Continued.

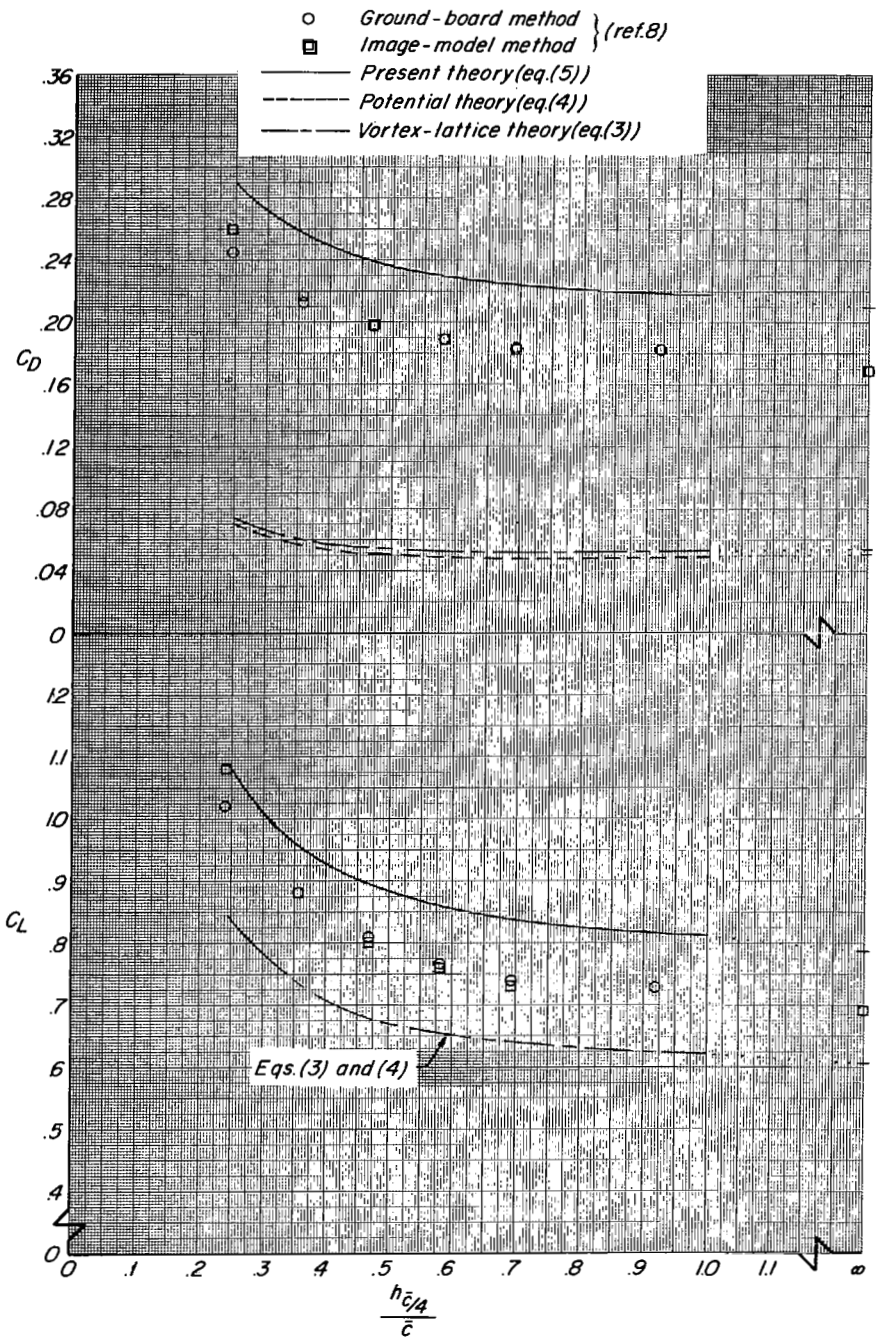

(c) $\Lambda = 60^0$; AR = 2.309.

Figure 2.- Continued.

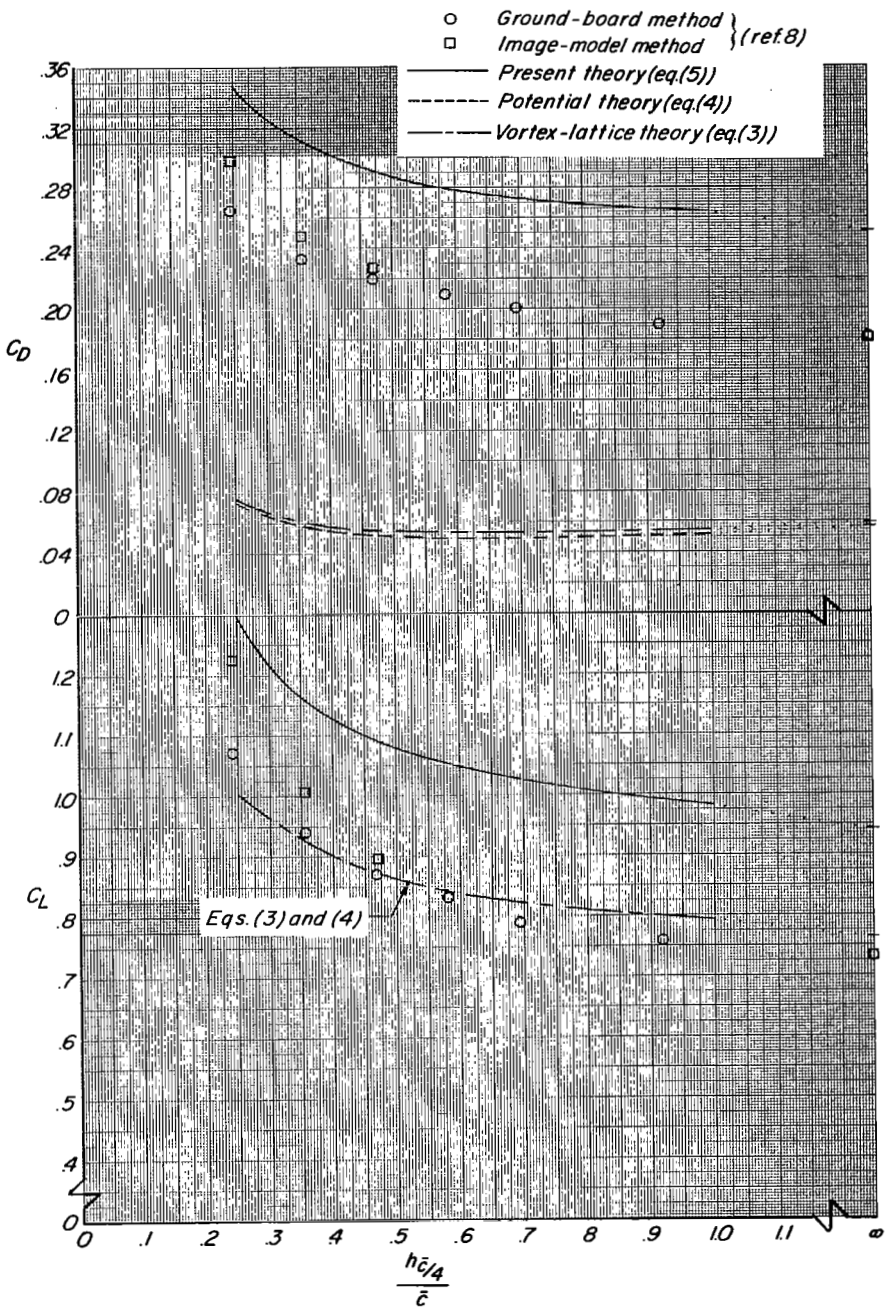

(d) $\Lambda = 50^{\circ}$; $AR = 3.356$.

Figure 2.- Concluded.

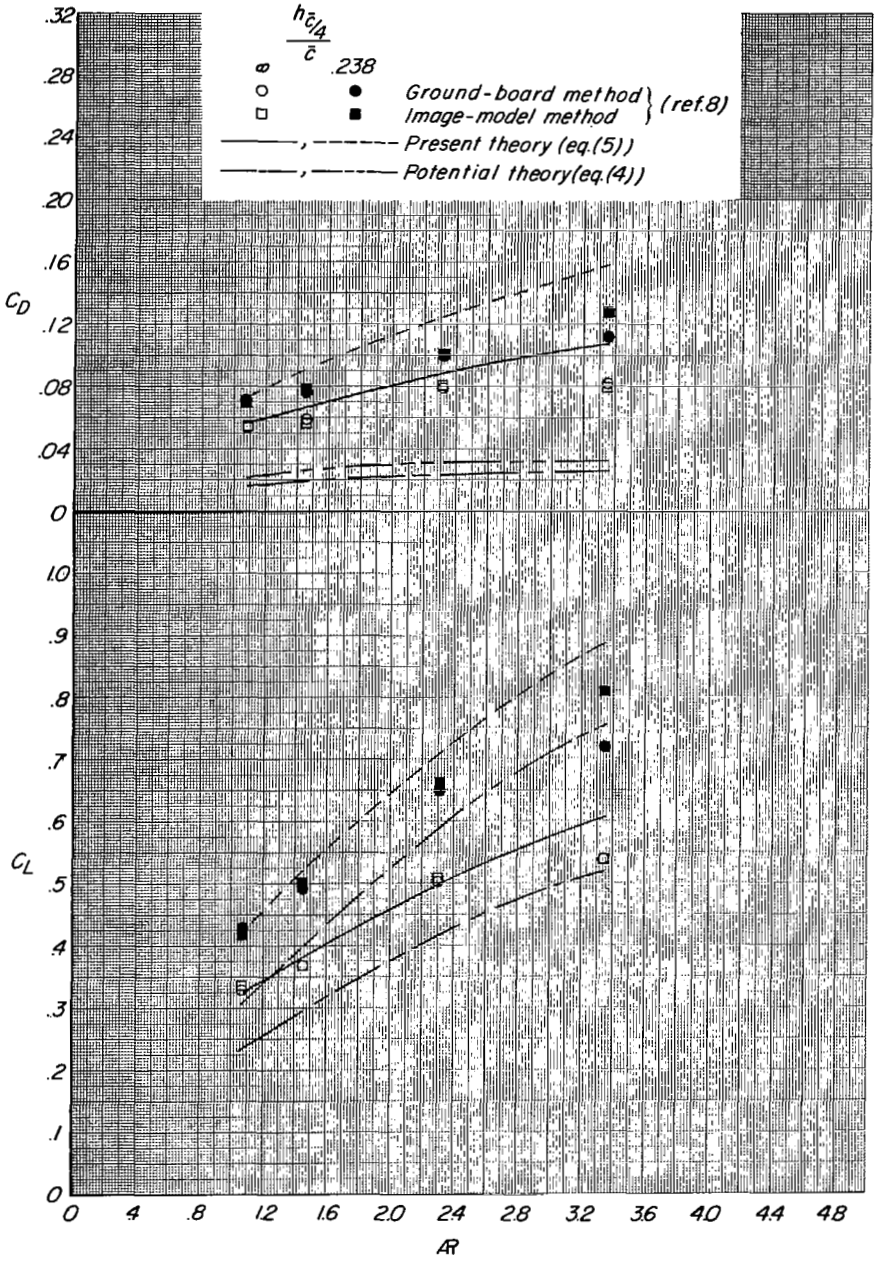

Figure 3.- Effect of aspect ratio on theoretical predictions of lift and drag coefficients at two heights above the ground and comparison with experimental data of reference 8. $\alpha = 10^0$.

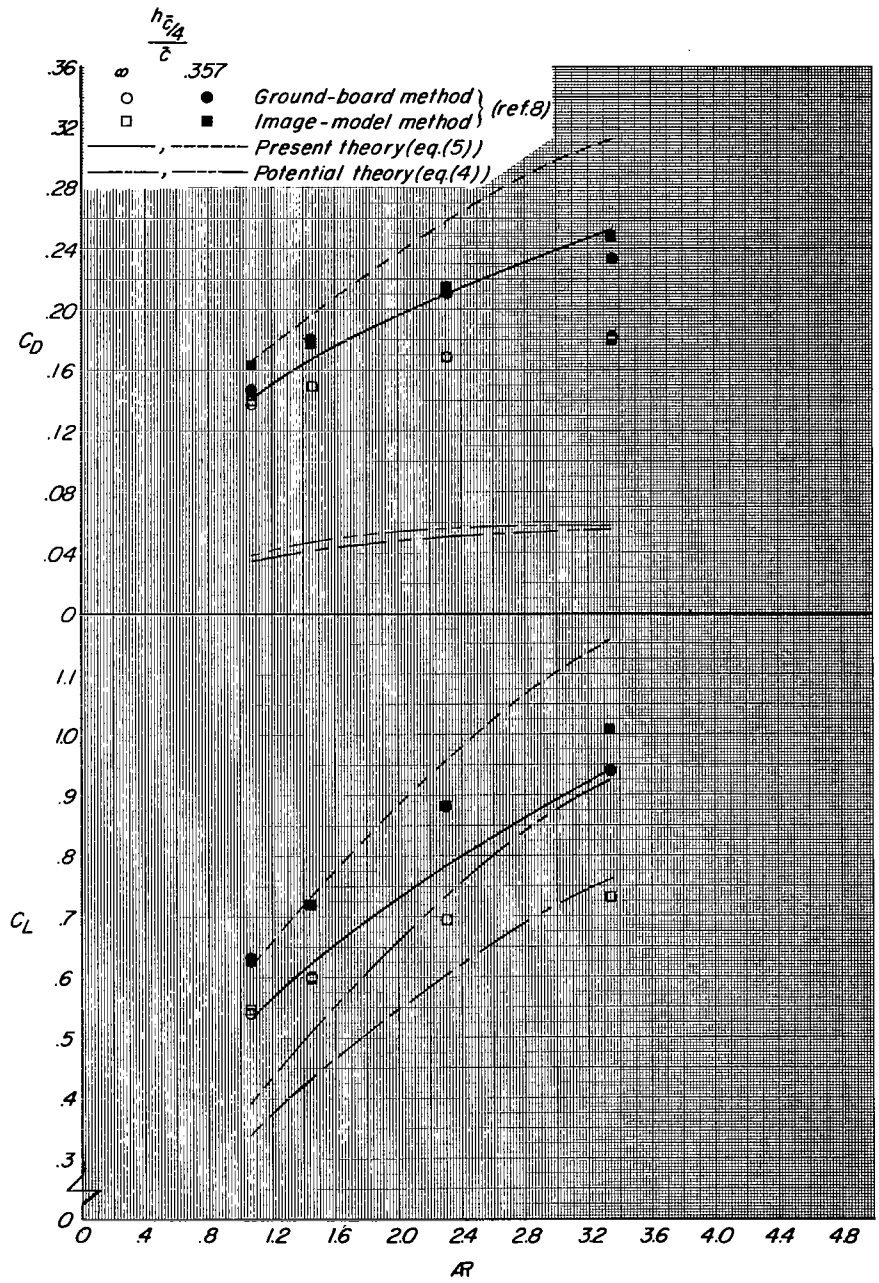

Figure 4.- Effect of aspect ratio on theoretical predictions of lift and drag coefficients at two heights above the ground and comparison with experimental data of reference 8. $\alpha = 15^0$.

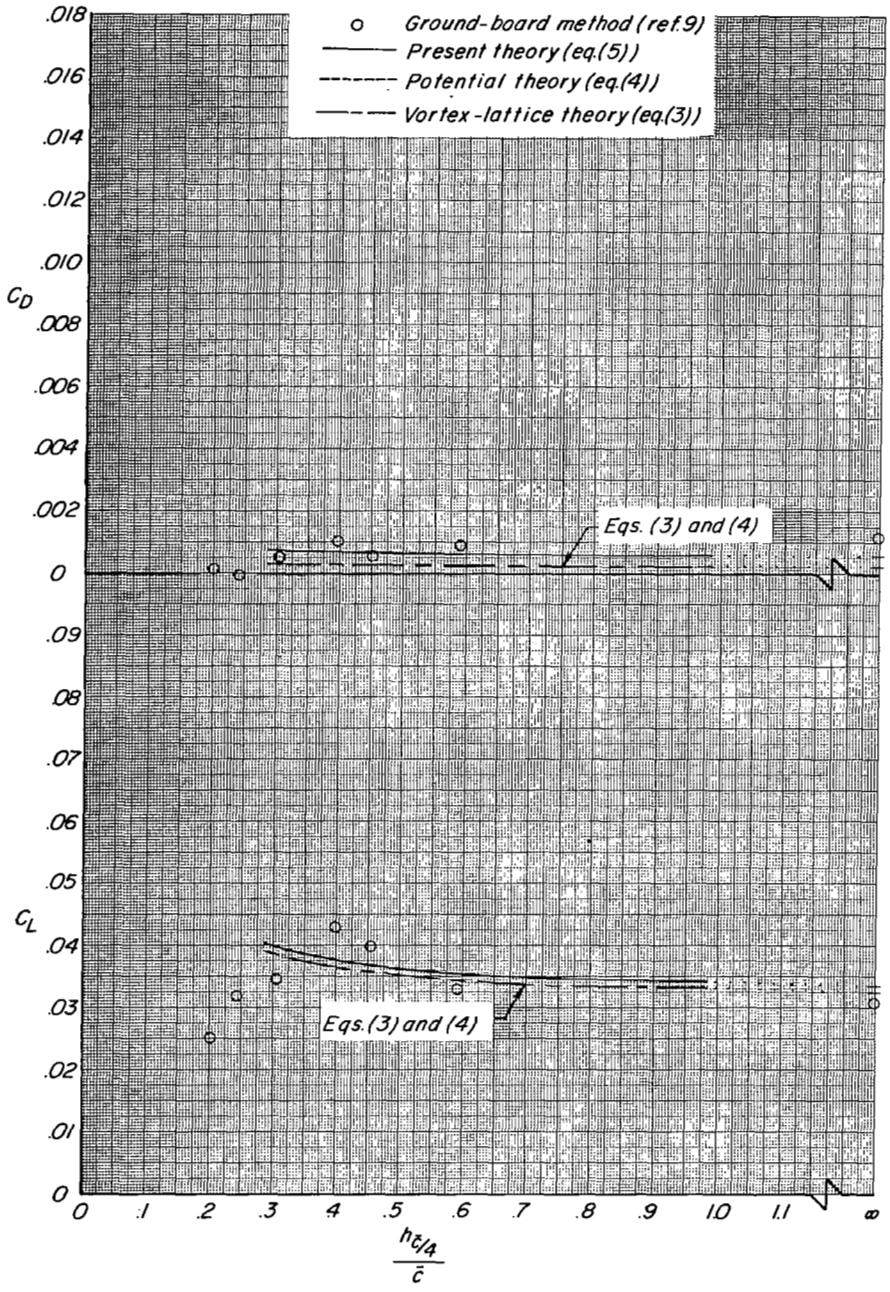

(a) $\alpha = 1^{\circ}$. Note the enlarged C_L and C_D scales.

Figure 5.- Comparison of lift and drag coefficients determined by different theories with the experimental data of reference 9. $\Lambda = 68^{\circ}$; AR = 1.616.

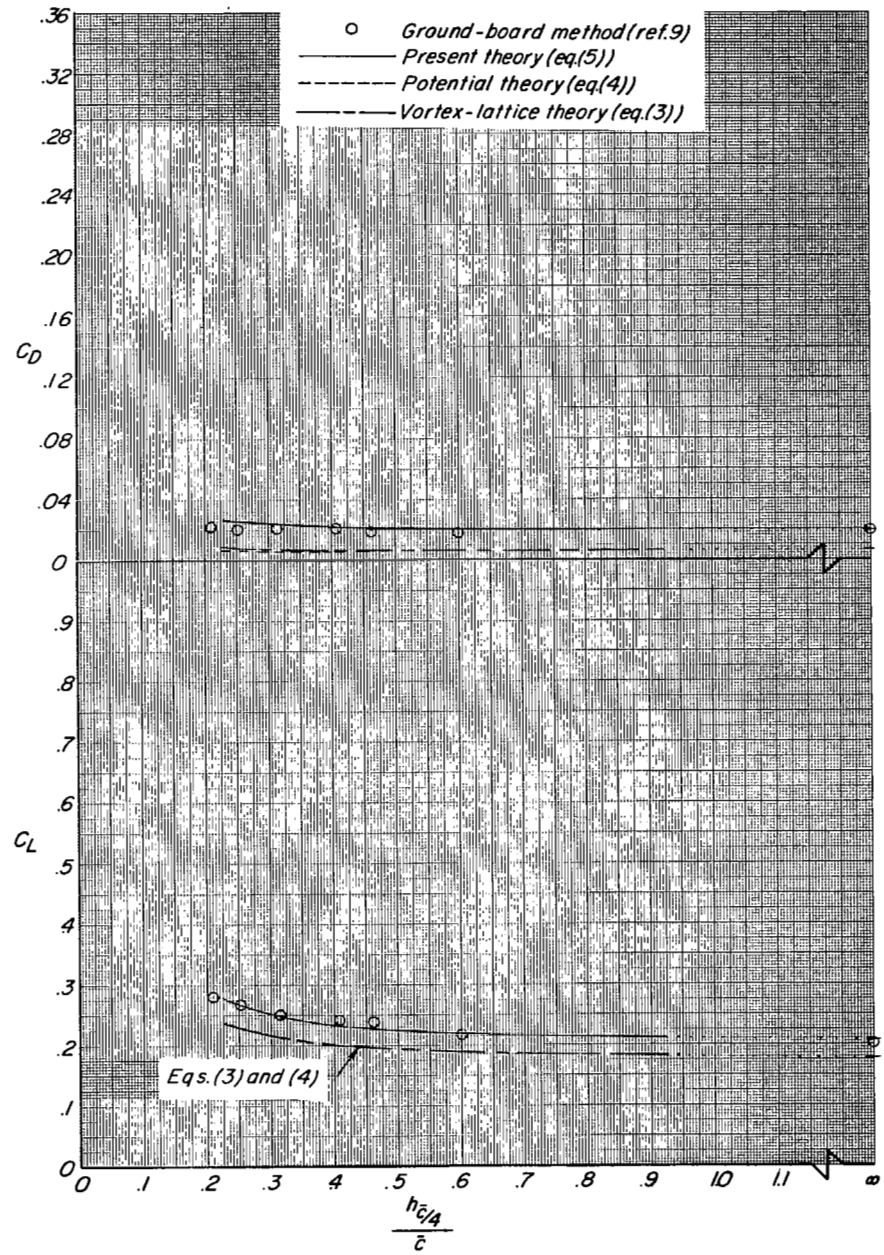

(b) $\alpha = 5.52^{0}$.

Figure 5.- Continued.

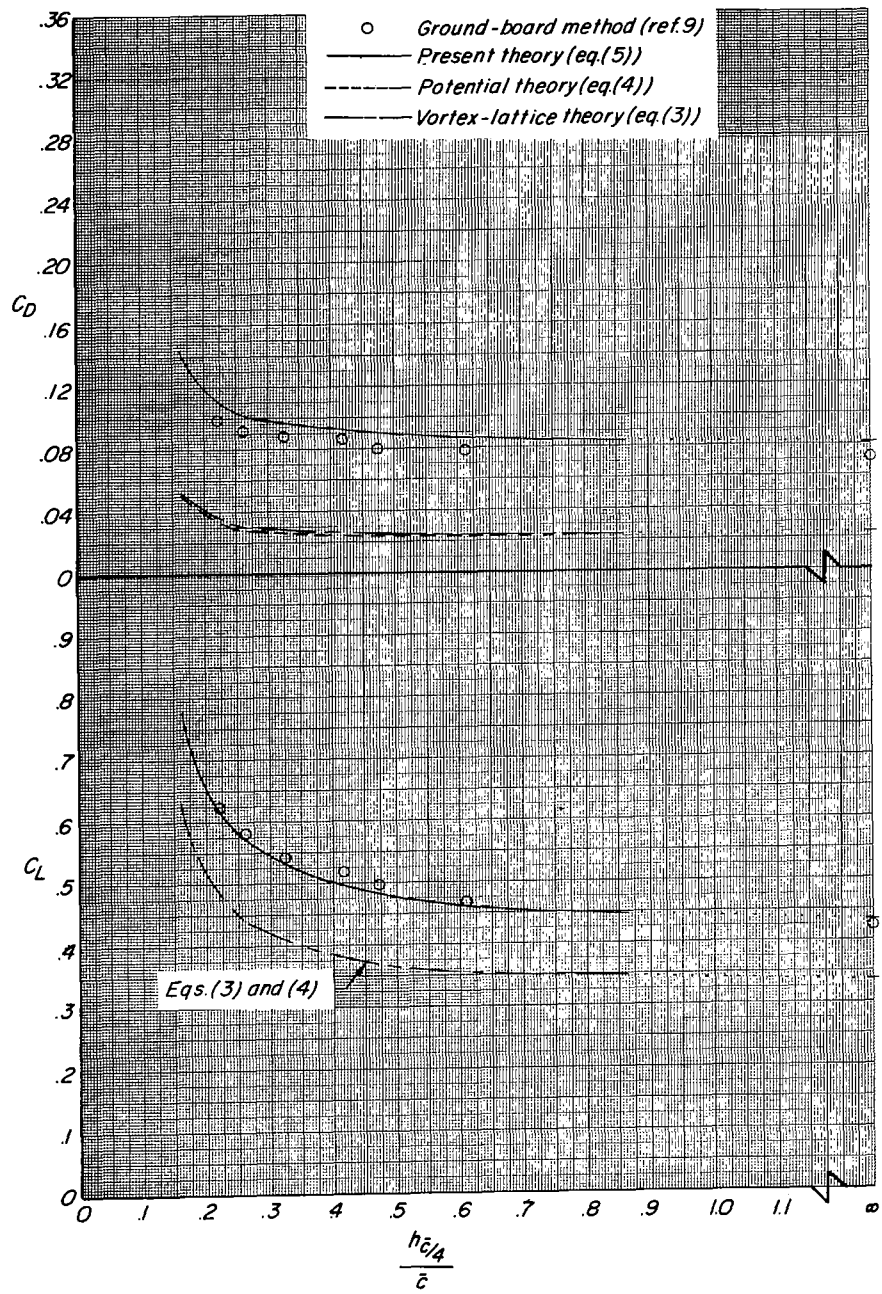

(c) $\alpha = 10.53^0$.

Figure 5.- Continued.

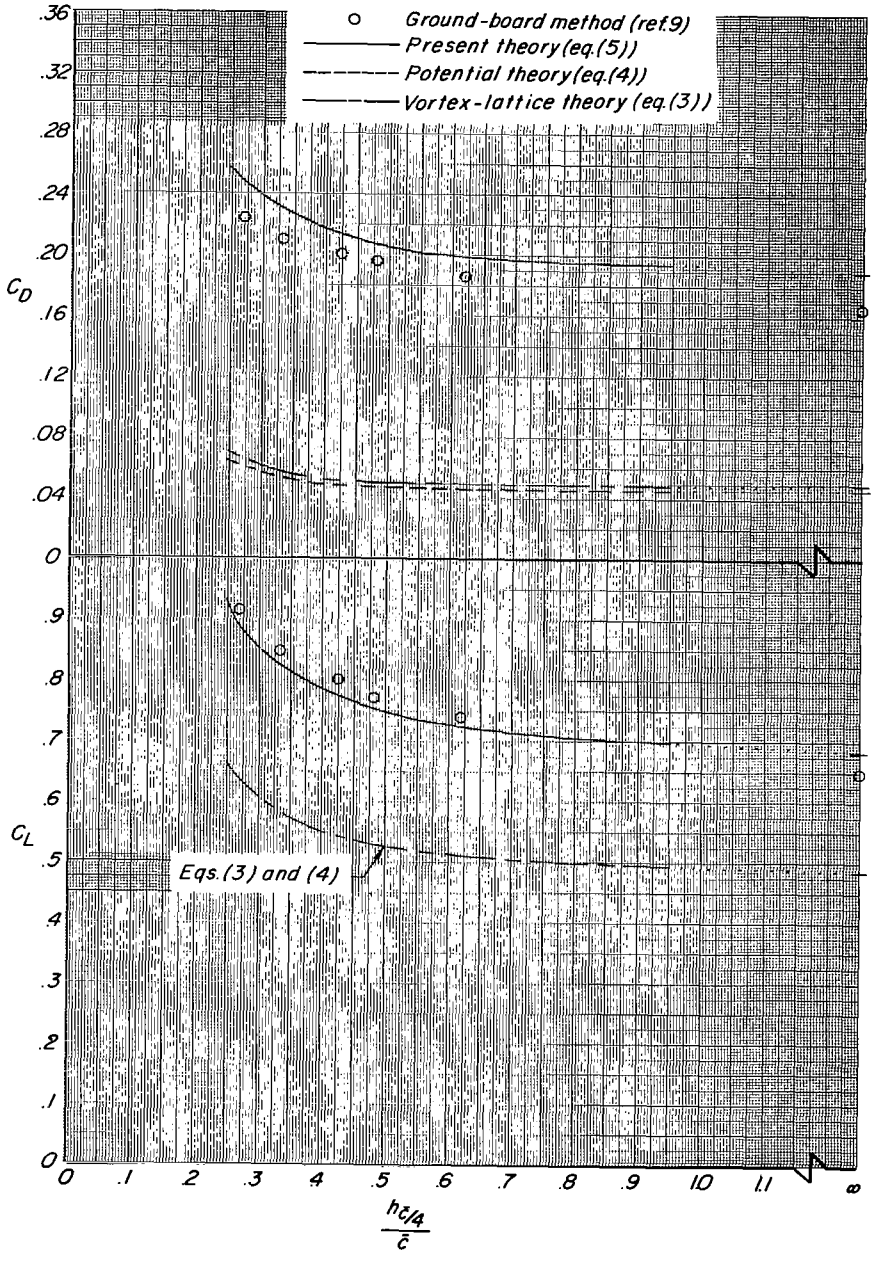

(d) $\alpha = 15.55^0$.

Figure 5.- Concluded.

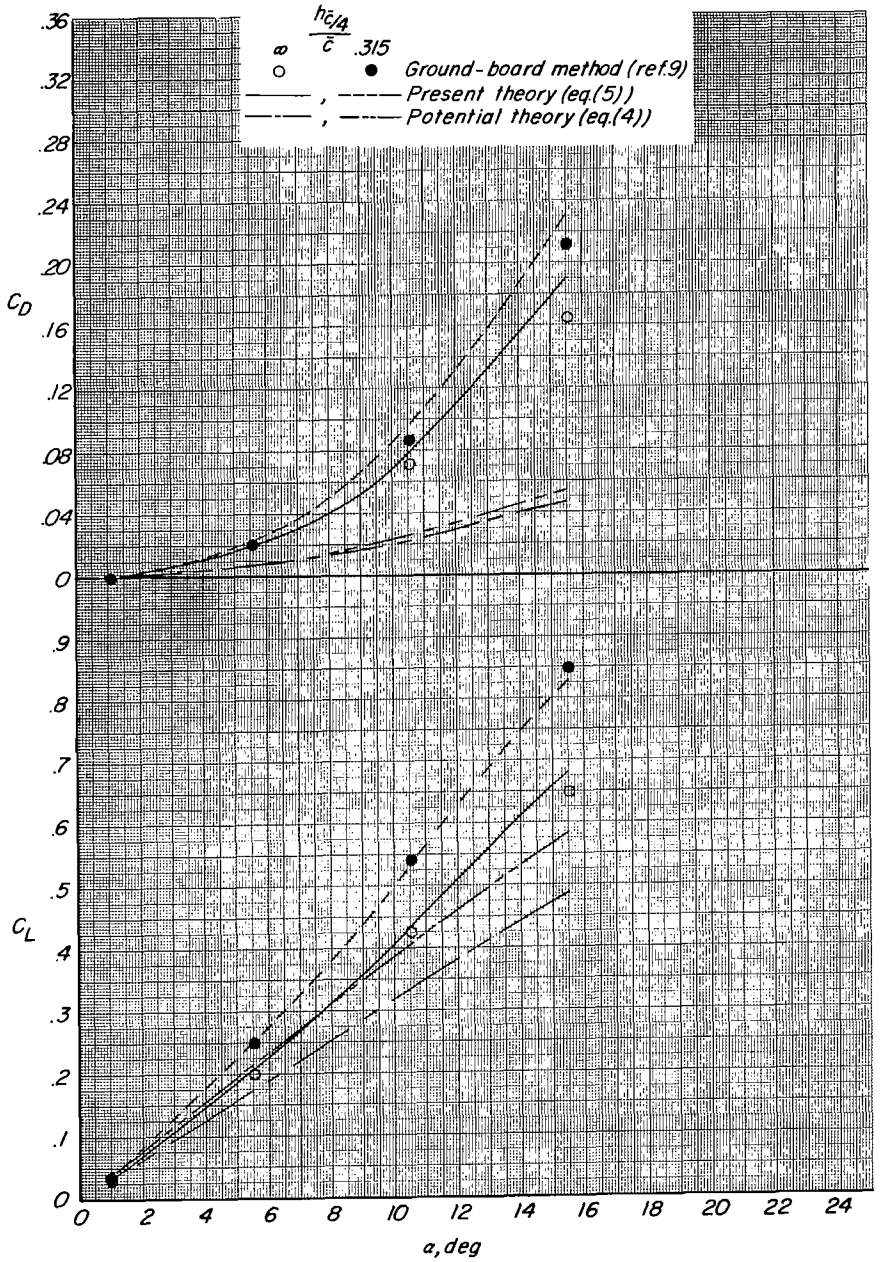

Figure 6.- Effect of angle of attack on theoretical predictions of lift and drag coefficients at two heights above the ground and comparison with data of reference 9. $\Lambda = 68^{0}$; $AR = 1.616$.

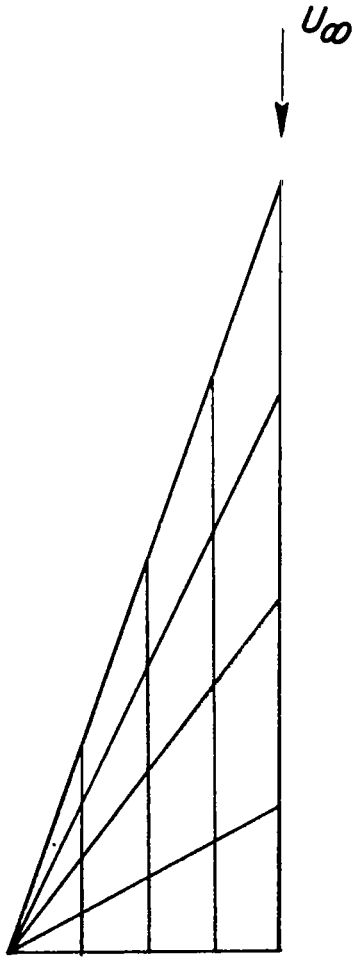

(a) Simplified vortex layout on left wing panel.

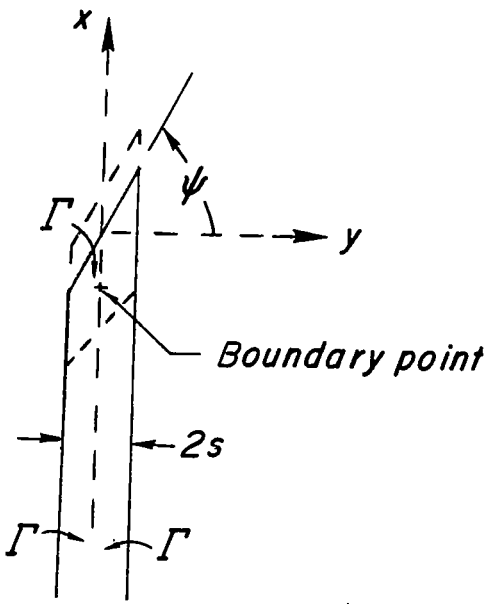

(b) Typical horseshoe-vortex layout. The positive z-direction is into the paper.

Figure 7.- Application of the vortex-lattice method to a delta-wing planform.

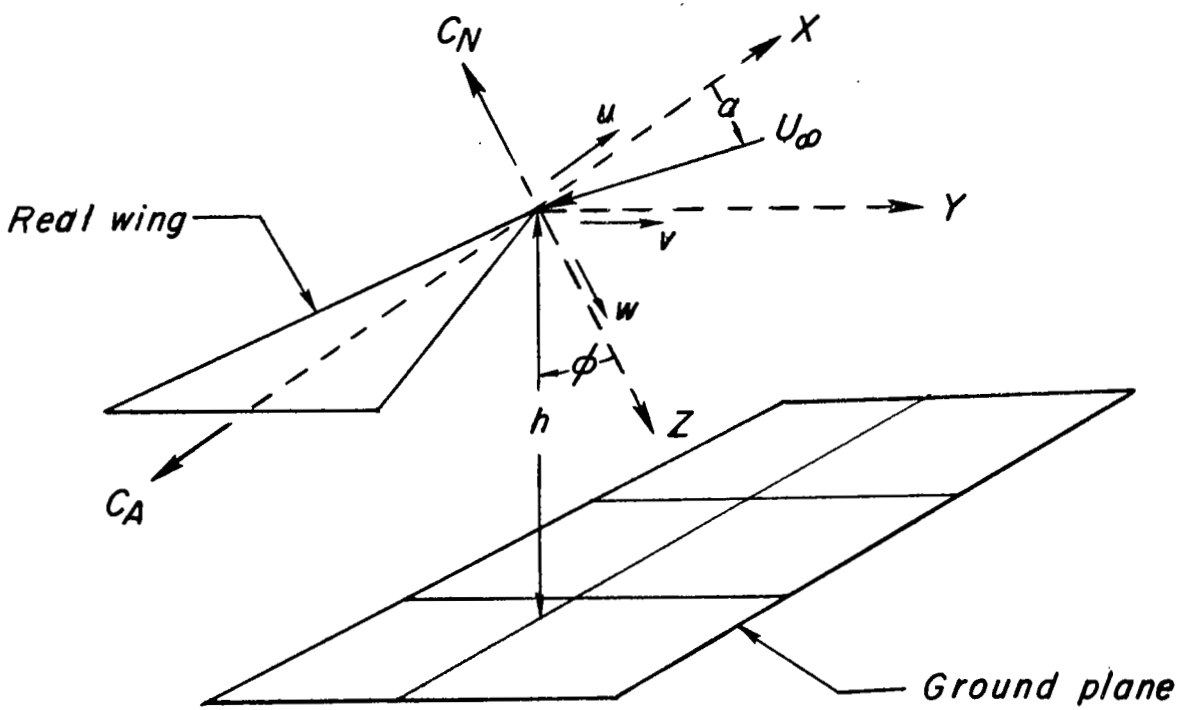

(c) Geometry associated with real wing.

Figure 7.- Continued.

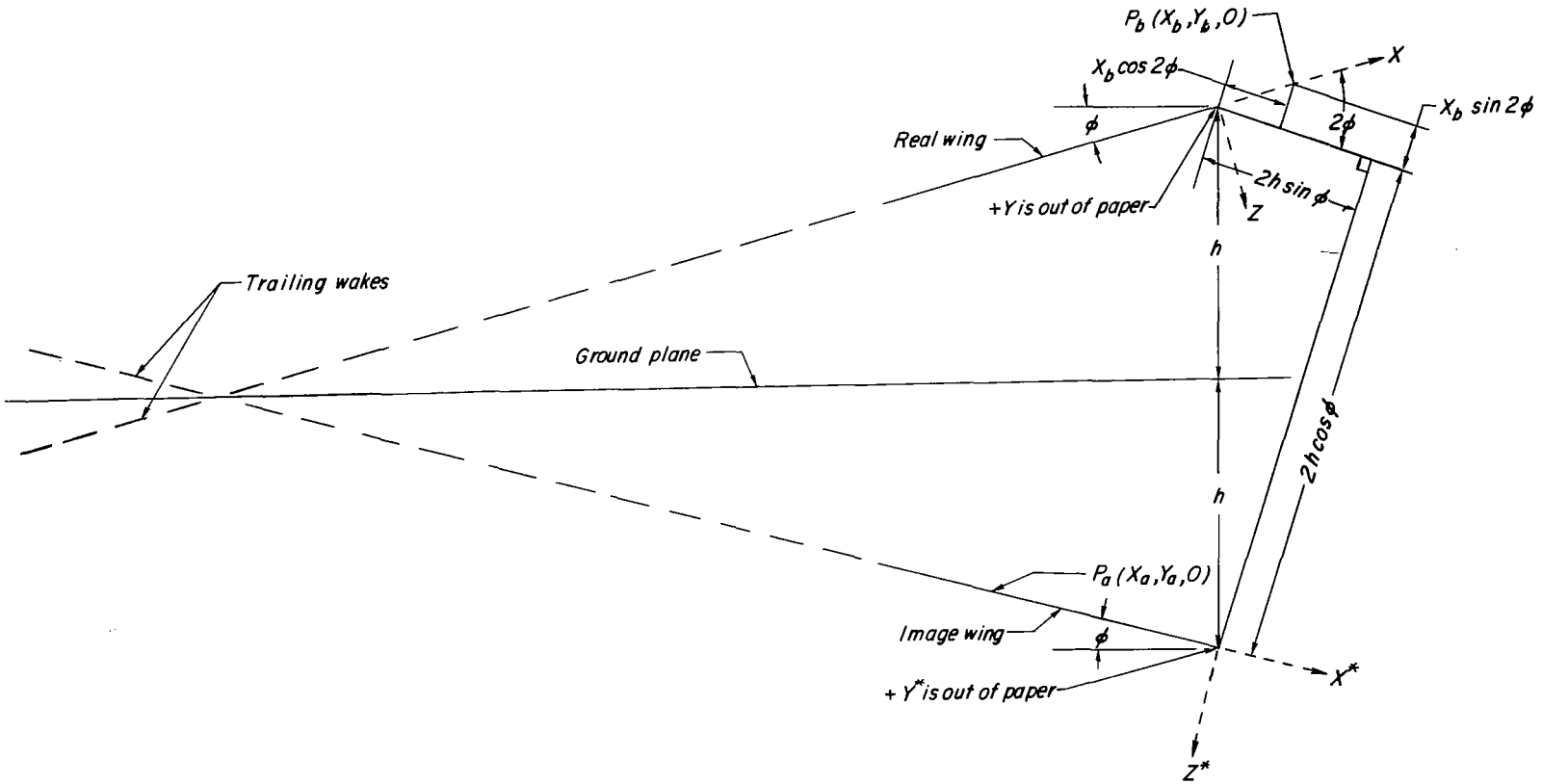

(d) Coordinate systems associated with real and image wings. Note that P_b is shown with X_b positive for clarity.

Figure 7.- Concluded.